
FewViewGS: Gaussian Splatting with Few View Matching and Multi-stage Training

Ruihong Yin
University of Amsterdam
r.yin@uva.nl

Vladimir Yugay
University of Amsterdam
v.yugay@uva.nl

Yue Li
University of Amsterdam
y.li6@uva.nl

Sezer Karaoglu
University of Amsterdam
3DUniversum
s.karaoglu@3duniversum.com

Theo Gevers
University of Amsterdam
3DUniversum
th.gevers@uva.nl

Abstract

The field of novel view synthesis from images has seen rapid advancements with the introduction of Neural Radiance Fields (NeRF) and more recently with 3D Gaussian Splatting. Gaussian Splatting became widely adopted due to its efficiency and ability to render novel views accurately. While Gaussian Splatting performs well when a sufficient amount of training images are available, its unstructured explicit representation tends to overfit in scenarios with sparse input images, resulting in poor rendering performance. To address this, we present a 3D Gaussian-based novel view synthesis method using sparse input images that can accurately render the scene from the viewpoints not covered by the training images. We propose a multi-stage training scheme with matching-based consistency constraints imposed on the novel views without relying on pre-trained depth estimation or diffusion models. This is achieved by using the matches of the available training images to supervise the generation of the novel views sampled between the training frames with color, geometry, and semantic losses. In addition, we introduce a locality preserving regularization for 3D Gaussians which removes rendering artifacts by preserving the local color structure of the scene. Evaluation on synthetic and real-world datasets demonstrates competitive or superior performance of our method in few-shot novel view synthesis compared to existing state-of-the-art methods.

1 Introduction

Reconstruction of a 3D scene representation from sparse 2D observations that can render novel views unseen during training has been an active field of research with wide applications in VR/AR and navigation. Recently, neural radiance fields (NeRF) [20] utilizing differentiable volume rendering and implicit scene representation achieved great results in novel view synthesis (NVS). The NeRF framework was extended to the sparse-view setting (few-shot NVS) using efficient training schemes, regularization losses, depth consistency, and image priors [11, 22, 8, 34]. While being good at rendering, NeRFs typically take a long time to be optimized, and their rendering speed is far from real-time which greatly limits their practical application.

3D Gaussian Splatting [13] has introduced an unstructured radiance field represented with 3D Gaussians. Gaussians are initialized from a sparse Structure-from-Motion (SfM) [29] point cloud and dynamically added or removed from the scene during training. With images observing a static scene from different viewpoints, Gaussian parameters are optimized using photometric loss. This method became widely adopted due to its training efficiency, unprecedented rendering speed, and quality. However, the rendering performance dramatically drops when fewer images are used for

training. While well-observed regions can be accurately rendered, less-supervised scene geometry is under-reconstructed, Gaussian parameters are overfitted to the views observing the scene [44], geometry artifacts [38] appear. In addition, optimization is highly dependent on the SfM initialization point cloud whose quality is also affected by the sparsity of the training views. There are several concurrent works exploring few-shot Gaussian splatting [15, 38, 24, 6, 46]. However, all of them rely on depth estimation [15, 38, 24, 6, 46] or diffusion priors [38]. In these methods, depth-estimation networks predict depth up to scale on unseen scenes, making them sensitive to domain shifts, while diffusion models increase training time.

In this paper, we introduce **FewViewGS**, a Gaussian splatting-based novel view synthesis method achieving state-of-the-art rendering results in a few-shot setup. We break the training process into the pre-training, intermediate, and tuning stages to better propagate the information to the novel views. During the pre-training stage, we use only training views to get a basic representation of the scene. This enables us to obtain a fundamental point cloud and scaled training view depth maps. In the intermediate stage, the emphasis is on optimizing the new perspectives. We use multi-view geometry and a novel view interpolation sampling to render unseen views coherent with the training images. For this, we match the pairs of training images, robustly warp the matches to the randomly sampled novel views between them, and enforce novel view consistency by applying geometry, color, and semantic losses. In the final stage, the scene representation undergoes refinement through a limited number of iterations, utilizing only the known views. During training, the 3D Gaussians are regularized by our proposed locality preserving regularization to maintain their local properties, eliminating the artifacts on the novel views. In summary, our **contributions** are as follows:

- A few-shot NVS Gaussian splatting-based system not relying on pre-trained depth estimation or diffusion models achieving SoTA rendering results.
- A multi-stage training scheme enabling seamless knowledge transfer from known to novel views.
- A robust warping-based novel view consistency constraint ensuring the coherence of the synthesized unseen images.
- 3D Gaussian locality preserving regularization handling visual artifacts.

2 Related work

Novel View Synthesis. Neural Radiance Fields [20] model a 3D scene using a neural network that takes the viewing direction and 3D location as input and predicts color and density. During training, the network is optimized to render the images of a scene from different angles. The network trained in such a fashion implicitly learns how to interpolate and extrapolate [39] to render the scene from the angles unseen during training at a very high resolution. Due to its capabilities, NeRF became widely adopted for 3D scene reconstruction [1, 18, 8, 34, 14], human body modeling [26, 25, 36, 16], robotics [41, 28], and medical imaging [7].

However, classical NeRFs require extensive training time and computational resources, making them less practical for real-time applications. There are several methods [2, 1, 21, 10, 42] focusing on efficiency by using multiscale scene representations [1] or efficient data structures for scene encoding [21, 10, 42, 2]. However, all those approaches come at the cost of lower rendering quality.

Recently introduced, 3D Gaussian Splatting [13] uses 3D Gaussians to represent the scene. To render a view of a scene, the 3D Gaussians in the camera frustum view are splatted to the image plane. Having several training images observing a static scene from different angles, the parameters of the 3D Gaussians are optimized by minimizing the photometric loss. Due to explicit geometry representation, this method achieves real-time rendering and fast optimization without compromising rendering quality. However, just as NeRF, Gaussian splatting requires multiple views observing the scene from various angles.

Few-shot Novel View Synthesis. Few-shot novel view synthesis aims to train a scene representation capable of generating new views of a scene using only a sparse number of training images. Due to the lack of multi-view constraints on the scene and usage of photometric losses, training such a representation remains challenging.

Several works explore how to train better NeRFs for the novel view synthesis in a sparse setting. One group of methods explores the regularization with priors from pre-trained neural networks [8, 34, 37]. For example, DSNeRF [8] and SparseNeRF [34] use depth regularization from pre-trained depth estimators on known views to guide optimization. DiffusioNeRF [37] uses weight regularization and priors from diffusion models.

Another line of work [4, 22, 11, 33, 31] focuses on imposing additional supervision on the novel views during training. For example, GeoAug [4] randomly samples novel views around the known frames and then calculates the color loss between the warped novel view and the known view. RegNeRF [22] designs depth smooth regularization on unobserved views. DietNeRF [11] argues that the high-level semantic information should be similar for individual scenes and proposes to apply semantic consistency loss on the novel views. SPARF [33] integrates multi-view correspondence and geometry loss to the optimization. ViP-NeRF [31] regularizes the network with visibility prior, which is generated by plane sweep volumes.

Simultaneously with our research, numerous methods have emerged focusing on few-shot Gaussian splatting for novel view synthesis. FSGS [46] proposes a Gaussian Unpooling strategy to generate dense Gaussians. SparseGS [38] adopts a floater removal strategy to remove unnecessary Gaussians close to the camera. DNGaussian [15], CoherentGS [24], DRGS [6] focus on regularizing the depth maps. Remarkably, all the few-shot novel view synthesis methods based on 3DGS try to integrate the pre-trained depth estimation networks in the pipelines.

Novel view regularization has shown great results in sparse novel view synthesis. However, sampling random novel views in the camera frustum can make the rendering results inconsistent. We therefore propose to use correspondences between the known views to regularize the novel views sampled between them robustly. Moreover, we avoid relying on complex priors. Using simple image matching in the 2D-pixel space, we avoid using depth estimation models predicting depth up to scale and heavy diffusion models which struggle on out-of-distribution datasets, while achieving state-of-the-art rendering results.

3 Method

The key idea of our approach is to enforce consistency between the sparse known views and the novel views in visually overlapping areas. As presented in Fig. 1, we introduce a multi-stage training scheme consisting of pre-training, intermediate, and tuning stages to gradually optimize the scene and obtain depth maps for the training views. After the pre-training stage, we start enforcing consistency of the novel views. For this, we first sample random training frames and match them with each other in pixel space. Further, we randomly sample a pose between the pairs of training frames and warp the matched pixels to it. We then filter out unreliable warped pixels and apply our new color, geometry, and semantic losses to the rendered novel view. This ensures the novel view remains consistent only in the regions that overlap with the known view pairs. In addition, we apply locality-preserving regularization to remove typical artifacts that appear in few-shot scenarios. We now outline our pipeline, beginning with an overview of Gaussian Splatting [13], followed by the novel view consistency mechanism, regularization losses, and our training scheme.

3.1 Preliminary

Gaussian splatting [13] is a recent radiance field representation that replaces the implicit neural network with explicit optimizable 3D Gaussians.

A single 3D Gaussian is parameterized by its mean $\mu \in \mathbb{R}^3$, covariance $\Sigma \in \mathbb{R}^{3 \times 3}$, opacity $o \in \mathbb{R}$, and a set of spherical harmonics coefficients $sh \in \mathbb{R}^{3(l+1)^2}$ with degree l for view-dependent color. The mean of a projected (splatted) 3D Gaussian in the 2D image plane μ_I is computed as follows:

$$\mu_I = \pi(P(T_{wc}\hat{\mu})) \quad , \quad (1)$$

where $\hat{\mu}$ denotes homogeneous mean, $T_{wc} \in SE(3)$ is the world-to-camera extrinsics, $P \in \mathbb{R}^{4 \times 4}$ is an OpenGL-style projection matrix, π is the projection to pixel coordinates. The 2D covariance Σ_I of a splatted Gaussian is computed as:

$$\Sigma_I = JR_{wc}\Sigma R_{wc}^T J^T \quad , \quad (2)$$

where $J \in \mathbb{R}^{2 \times 3}$ is the Jacobian of the affine approximation of the projective transformation, $R_{wc} \in SO(3)$ is the rotation component of T_{wc} . For further details on the splatting process, we refer to [47].

Parameters of the 3D Gaussians are iteratively optimized by minimizing the photometric loss between rendered and training images. During optimization, covariance is decomposed as $\Sigma = RSS^T R^T$, where $R \in \mathbb{R}^{3 \times 3}$ and $S = \text{diag}(s) \in \mathbb{R}^{3 \times 3}$ are rotation and scale respectively to preserve covariance

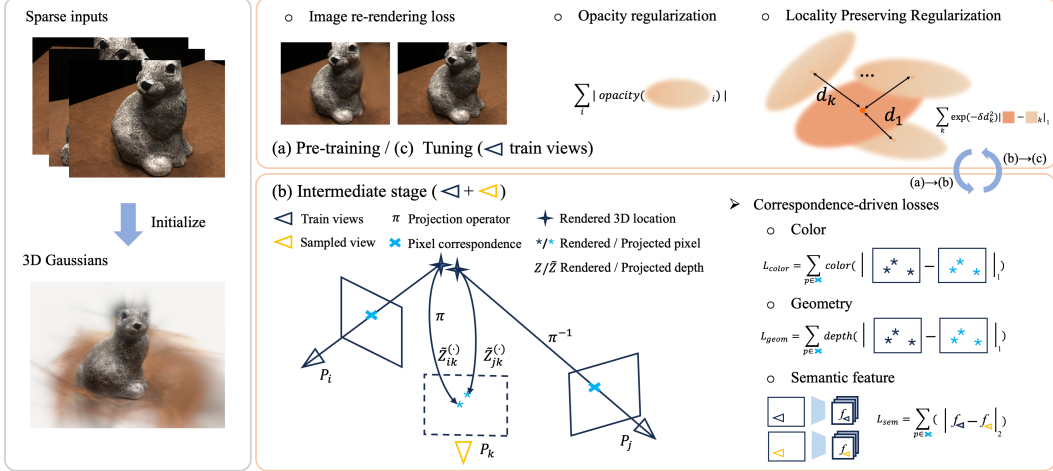


Figure 1: **FewViewGS pipeline.** Our method consists of a multi-stage training scheme of (a) pre-training, (b) intermediate, and (c) tuning stages. **Top right: pre-training / tuning.** At the beginning and end, Gaussians are optimized solely on the known input views, utilizing color re-rendering loss and regularization terms on total opacity and local appearance. **Bottom right: intermediate.** Correspondences are first extracted from the pairs of training images and projected onto the virtual sampled views. Given the projected and virtual renders, color, geometry, and semantic losses are calculated at the projected pixels in the new views.

positive semi-definite property. Color c for a pixel influenced by n ordered Gaussians is rendered as:

$$c = \sum_{i=1}^n c_i \cdot \alpha_i \cdot T_i, \text{ with } T_i = \prod_{j=1}^{i-1} (1 - \alpha_j), \quad (3)$$

with c_i the color of i^{th} Gaussian and α_i computed as:

$$\alpha_i = o_i \cdot \exp(-\sigma_i) \quad \text{and} \quad \sigma_i = \frac{1}{2} \Delta_i^T \Sigma_{I,i}^{-1} \Delta_i, \quad (4)$$

where $\Delta_i \in \mathbb{R}^2$ is the offset between the 2D mean of a splatted Gaussian and the pixel coordinate. Similarly, this blending process could be extended to render pixel depth. We compute the depth d of a pixel that is influenced by n ordered Gaussians as:

$$d = \sum_{i=1}^n \mu_i^z \cdot \alpha_i \cdot T_i, \quad (5)$$

where μ_i^z is the z component of the mean, α_i and T_i are the same as in Eq. (3).

This splatting approach provides significantly faster training and inference time with no compromise on rendering quality compared to NeRF. During training, new Gaussians are added and removed from the scene based on the heuristics introduced in [13] to improve the scene coverage.

3.2 Novel View Consistency

Our main goal is to ensure the novel views are consistent with the training views in overlapping regions, maintaining visual coherence. However, determining which specific pixels in the training views should match those in the novel views is challenging.

Other few-shot methods [4, 22, 11, 33, 31] try to address this by randomly sampling novel views within the viewing frustum of a training frame and then applying regularization techniques to them. In contrast, our approach uses pairs of training views to more robustly identify which pixels need regularization in the novel views. This method enhances accuracy and consistency, aligning novel views more effectively with the training data, resulting in higher quality and more coherent visual output.

As the first step, for a pair of training images i and j we find the pixel correspondences C_i, C_j using a robust image matcher [9]. Since the training views' poses P_i and P_j are known, a novel view pose P_k is randomly sampled between them. Further, we render the depth maps of the matched pixels Z_i, Z_j of the training views, and warp them to the novel view, defined by:

$$C_{u,i} = \pi(P_k \cdot \pi^{-1}(C_i, Z_i)), \quad (6)$$

where $C_{u,i}$ are the pixels of the novel view, π and π^{-1} are the projections from 3D to 2D and from 2D to 3D respectively.

Having projected the matched pixels to the novel view, they are used to supervise novel view synthesis by applying color, geometric, and semantic losses. However, natural errors stemming from color and depth rendering, or image matching, make supervision over all the projected pixels unstable. To mitigate these effects, an agreement masking is proposed and defined as follows:

$$M(x_i, x_j, \theta) = I(|x_i^k - x_j^k| < \theta), \quad (7)$$

where x_i, x_j are image-shape matrices, $\theta \in R$ is an agreement threshold, and I is an indicator function.

In addition, the warped values often end up in the wrong locations when warped from the high color gradient regions, contaminating the losses. This happens mostly because of inaccurate matches in such areas. To address this, we introduce a color gradient weighting W which alleviates the effect of errors in texture-rich regions. For a color gradient G at a pixel (u, v) , it is computed as:

$$W(G_{u,v}, \theta_{grad}) = \begin{cases} \exp(-G_{u,v}) & \text{if } |G_{u,v}| > \theta_{grad} \\ 1 & \text{else} \end{cases} \quad (8)$$

where $|G_{u,v}|$ is gradient magnitude, θ_{grad} is a scalar threshold.

Denoting matches between known images i and j as $P_{i,j}$, we enforce the geometric consistency of the novel view using the loss:

$$L_{geom} = \sum_{p \in P_{i,j}} M(\tilde{Z}_{ik}^p, \tilde{Z}_{jk}^p, \theta_g) \cdot W(G_t^p, \theta_{grad}) \cdot \min(|Z_k^p - \tilde{Z}_{ik}^p|_1, |Z_k^p - \tilde{Z}_{jk}^p|_1), \quad (9)$$

where Z_k^p is the rendered depth of a novel view k at a pixel p , $\tilde{Z}_{ik}^p, \tilde{Z}_{jk}^p$ are the projected depth values from the known views i and j respectively, θ_g is an agreement threshold. t is set to i if $|Z_k^p - \tilde{Z}_{ik}^p|_1$ is less than $|Z_k^p - \tilde{Z}_{jk}^p|_1$ and to j otherwise. We take the minimum over the pair of depth discrepancy to further reduce the influence of inaccurate projections.

To regularize the appearance of the novel view, the loss in the color space is applied as follows:

$$L_{color} = \sum_{p \in P_{i,j}} M(\tilde{Z}_{ik}^p, \tilde{Z}_{jk}^p, \theta_g) \cdot W(G_t^p, \theta_{grad}) \cdot \min(|c_k^p - \tilde{c}_{ik}^p|_1, |c_k^p - \tilde{c}_{jk}^p|_1), \quad (10)$$

where c_k^p is the rendered color of a novel view k at pixel p . t is defined following the same logic as in Eq. (9).

Finally, the novel view should have similar semantics to the training views in the overlapping regions. Since pre-trained deep neural networks can encode semantic information of the images [30, 27, 23], the loss is added on the feature space of the novel views:

$$L_{sem} = \sum_{p \in P_{i,j}} M(\tilde{Z}_{ik}^p, \tilde{Z}_{jk}^p, \theta_g) \cdot W(G_t^p, \theta_{grad}) \cdot \min(|f_k^p - f_i^p|_2, |f_k^p - f_j^p|_2), \quad (11)$$

where f_i, f_j, f_k are image-sized features extracted with a pre-trained network from the views i, j, k respectively. t is defined following the same logic as in Eq. (9).

The final equation for the novel view consistency loss is expressed as:

$$L_{consistency} = \alpha \cdot L_{geom} + \beta \cdot L_{color} + \gamma \cdot L_{sem}, \quad (12)$$

where α, β, γ are the respective scalar weights.

3.3 Locality Preserving Regularization

After examining optimized 3D scenes in a few-shot setting, it was found that accurate rendering results from Gaussian splatting occur when color values are smooth within local neighborhoods. However, in a standard setting, the photometric loss does not explicitly enforce this. Although this is not an issue when numerous frames are available, it leads to artifacts in a few-shot setup.

Therefore, a locality-preserving regularization is proposed to address this issue. For every Gaussian i , its neighborhood N_i is defined by finding the K nearest neighbors in 3D space. Furthermore, the color parameters of Gaussian i are enforced to be proportionally closer to those of its neighborhood:

$$L_{locality} = \sum_{k \in N_i} \exp(-\delta \cdot |\mu_k - \mu_i|_2) \cdot |c_k - c_i|_2, \quad (13)$$

where δ is a scaling factor, c_i and c_k are the colors of the Gaussian i and its neighbor k respectively. The weight function $\exp(-\delta \cdot |\mu_k - \mu_i|_2)$ measures the influence of the neighbor colors based on their distance to the Gaussian center. The effect of locality regularization is demonstrated quantitatively in Tab. 4 and qualitatively in Tab. 2.

3.4 Multi-stage Training Scheme

Our training scheme serves two goals. First, to avoid overfitting to the training views and to provide a coarse initialization for synthesizing novel views. Second, to provide scaled depth estimates for the training views to allow warping.

During the pre-training stage, only the training views are used to optimize the 3D Gaussians for a small number of iterations using the loss:

$$L_{pre-training} = \lambda \cdot L_{photometric} + \chi \cdot L_{opacity} + \zeta \cdot L_{locality}, \quad (14)$$

where $L_{photometric}$ is the photometric loss from [13], $L_{opacity}$ is the $L2$ regularization term for the Gaussians' opacity, and λ, χ, ζ are the scalar weights. Opacity regularization [32] is added to remove the unobserved floating Gaussians that cause floating artifacts.

In the intermediate stage, novel views are synthesized and used as supervision for the Gaussians to avoid overfitting. We found that sparse supervision from feature matching and noise in pseudo labels for novel views leads to model collapse in certain scenes. To address this, training views are also used to regularize the scene representation, with a downscaled $L_{pre-training}$. Since the depth maps become available after the pre-training stage, we start using novel view consistency losses as described in Sec. 3.2:

$$L_{intermediate} = \kappa \cdot L_{consistency} + \eta \cdot L_{pre-training}, \quad (15)$$

where κ, η are the scalar weights for the respective losses.

The tuning stage is designed to refine the network using ground truth, provide supervision for unmatched pixels during the intermediate phase, and reduce the impact of noise in novel views. At the same time, it is crucial not to overfit the training views. Only training views are used for optimizing the $L_{pre-training}$ loss for a small number of iterations.

4 Experiments

Here we describe our experimental setup and then evaluate our approach against state-of-the-art few-shot NVS methods on commonly used datasets [12, 19, 20]. In addition, we compare our method with concurrent works. The tables highlight best results as **first**, **second**, **third**. Concurrent works in the tables are marked with an asterisk*.

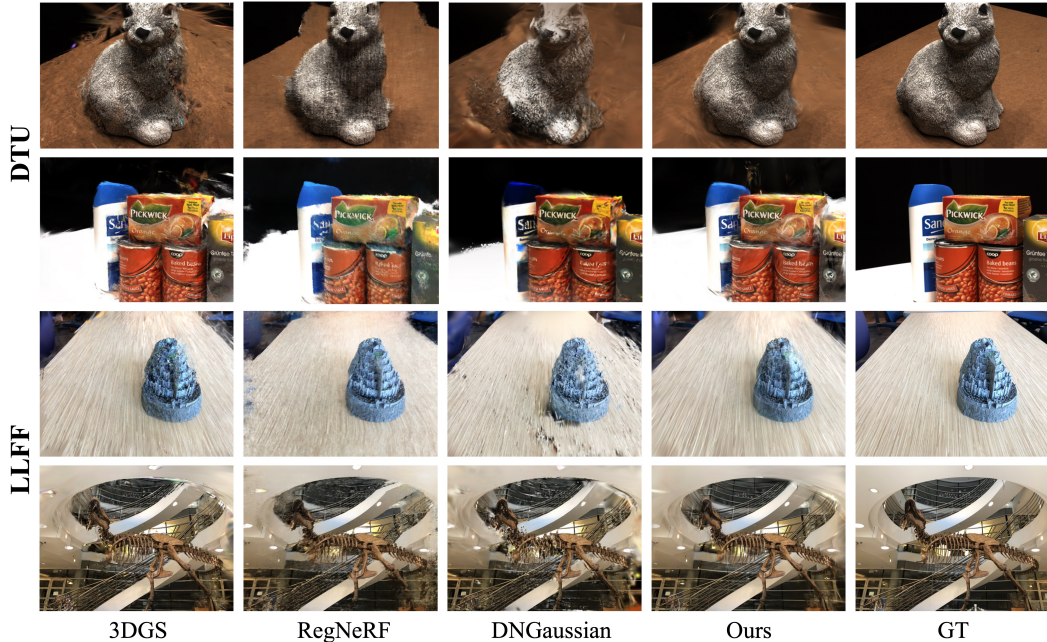


Figure 2: **Qualitative comparison on DTU [12] and LLFF [19] datasets.** The results show that RegNeRF tends to produce blurred outcomes. 3DGS and DNGaussian introduce artifacts in the novel view. In contrast, our method generates better qualitative results.

4.1 Setup

Datasets. Our approach is evaluated on commonly used real-world [12, 19] and synthetic [20] datasets. Following previous methods, 15 scenes are selected on the DTU [12] dataset in our experiments, in which the background is removed during evaluation. LLFF [19] dataset is composed of 8 real-world scenes. Following FreeNeRF [40], we choose the 8th image for inference and then uniformly sample sparse views from the remaining images as the training set. For both datasets, the training set consists of 3 views. We use $\frac{1}{4}$ resolution images on DTU and $\frac{1}{8}$ resolution on LLFF. Synthetic Blender dataset [20] contains 8 scenes. We use the same setup as in [11].

Evaluation Metrics. We use PSNR [35], SSIM, and LPIPS [45] to measure rendering performance. For LPIPS, a lower value denotes better performance, while a higher value is preferable for PSNR and SSIM. Our method is compared to NeRF-based and concurrent 3DGS-based methods, including NeRF[20], SRF [5], PixelNeRF [43], MVNeRF [3], Mip-NeRF [1], DietNeRF [11], RegNeRF [22], FreeNeRF [40], SparseNeRF [34], 3DGS [13], DNGaussian [15], FSGS [46], DRGS[6], and SparseGS [38].

Implementation details. Our method is trained for 10000 iterations in total on all the datasets. We use the same schedule by spending 2000 iterations on the pre-training stage, 7500 on the intermediate stage, and 500 on the tuning stage. In the pre-training stage and tuning stages, loss weights $\{\lambda, \chi, \zeta\}$ are set to $\{1.0, 0.001, 0.001\}$ respectively. In the intermediate stage, geometry, color, and semantic loss weights α, β, γ are set to 0.5, 0.05, and 0.001. Consistency and pre-training loss weights κ, η are set to 1.0 and 0.05. δ in the locality preserving regularization is set to 2.0. The gradient threshold θ_{grad} is 0.1. θ in the agreement masking is 10.0. We use a pre-trained VGG16 to extract semantic features. The experiments are run on one NVIDIA A6000 GPU.

4.2 Quantitative Results

We report our rendering performance on commonly used real-world datasets in Tab. 1. We compare our method against NeRF-based methods and concurrent Gaussian-based approaches (marked with an asterisk *). Our method performs on par or better than most of the presented approaches significantly improving over the baseline. On the DTU dataset, FreeNeRF [40] performs slightly better since it hallucinates over the missing regions, while Gaussian Splatting can't due to its explicit geometry

Table 1: **Quantitative evaluation on DTU[12] and LLFF[19].** We use 3 training views across all the datasets. Concurrent works are marked with an asterisk*.

Setting	DTU			LLFF		
	PSNR \uparrow	SSIM \uparrow	LPIPS \downarrow	PSNR \uparrow	SSIM \uparrow	LPIPS \downarrow
SRF[5]	15.32	0.671	0.304	12.34	0.250	0.591
PixelNeRF[43]	16.82	0.695	0.270	7.93	0.272	0.682
MVNeRF[3]	18.63	0.769	0.197	17.25	0.557	0.356
Mip-NeRF[1]	8.68	0.571	0.353	14.62	0.351	0.495
DietNeRF[11]	11.85	0.633	0.314	14.94	0.370	0.496
RegNeRF[22]	18.89	0.745	0.190	19.08	0.587	0.336
FreeNeRF[40]	19.92	0.787	0.182	19.63	0.612	0.308
SparseNeRF[34]	19.55	0.769	0.201	19.86	0.624	0.328
3DGS[13]	16.94	0.816	0.152	19.48	0.664	0.220
DRGS[6]*	-	-	-	17.17	0.497	0.337
SparseGS[38]*	18.89	0.702	0.229	-	-	-
DNGaussian[15]*	18.23	0.780	0.184	18.86	0.600	0.294
FSGS[46]*	-	-	-	20.43	0.682	0.248
Ours (Rand. Init.)	19.13	0.792	0.186	18.96	0.585	0.307
Ours	19.74	0.861	0.127	20.54	0.693	0.214

Table 2: **Qualitative evaluation.** We compare rendering with (*w*) and without (*w/o*) locality regularization, clearly indicating its effectiveness.

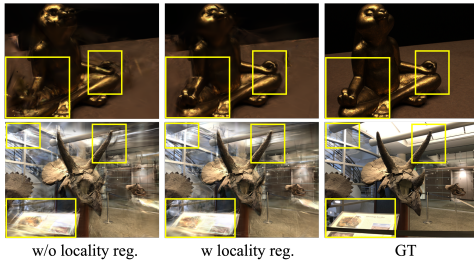


Table 3: **Quantitative evaluation on Blender[20] dataset.** FewViewGS shows superior performance using 8 training views.

Method	PSNR \uparrow	SSIM \uparrow	LPIPS \downarrow
NeRF[20]	14.934	0.687	0.318
DietNeRF[11]	23.147	0.866	0.109
FreeNeRF[40]	24.259	0.883	0.098
SparseNeRF[34]	22.410	0.861	0.119
3DGS[13]	22.226	0.858	0.114
DNGaussian[15]*	24.305	0.886	0.088
Ours	25.550	0.886	0.092

encoding. Our method shows SoTA results on LLFF datasets. Interestingly, our method shows compelling results even with random Gaussian initialization. Finally, our method shows state-of-the-art results on the synthetic Blender dataset in Tab. 3.

4.3 Ablation Study

We ablate over our key design choices presented in the paper on the DTU dataset with 3 training views in Tab. 4, in which random initialization is used for 3D Gaussians. In the ablations, the effects of each contribution are examined in isolation.

Locality Preserving Regularization. The locality preservation loss improves rendering when added standalone to the vanilla Gaussian Splatting (row *ii*) and when added to the consistency losses in a multi-stage training setup (row *xiv*).

Novel View Consistency. We ablate over novel view consistency losses and show our results in rows *iii* to *ix*. First, it is shown in rows *iii* to *v* that geometry, appearance, and semantic losses contribute to the higher quality rendering when added separately. In particular, geometry and color consistency remarkably improve the performance, since they directly influence the attributes of 3D Gaussians and are highly related to the view-synthesis task. In rows *iii*, *iv*, *v* it is shown that all three consistency losses lead to even better results. Experiments are conducted on different large-scale feature extraction backbones for the semantic loss, such as DINOv2 [23], CLIP [27], and VGG [30] in *vii*, *viii*, *ix*. The results demonstrate that DINOv2 and CLIP perform worse than VGG. This occurs because DINO and CLIP significantly down-sample features early in their encoders, leading to missing details and blurring, especially in the boundary regions, as illustrated in Fig. 6. In contrast, our method utilizes

Table 4: **Ablation study on DTU [12] dataset under 3-view setting.**

	Method	PSNR \uparrow	SSIM \uparrow	LPIPS \downarrow
i	3DGS [13]	15.04	0.676	0.246
ii	$L_{locality}$	15.64	0.683	0.243
iii	L_{geom}	18.17	0.736	0.198
iv	L_{color}	18.50	0.773	0.192
v	L_{sem}	15.52	0.691	0.235
vi	$L_{geom} + L_{color}$	18.87	0.791	0.186
vii	$L_{geom} + L_{color} + L_{sem}$ (DINOv2 [23])	18.71	0.787	0.188
viii	$L_{geom} + L_{color} + L_{sem}$ (CLIP [27])	17.86	0.762	0.200
ix	$L_{geom} + L_{color} + L_{sem}$ (VGG [30])	18.95	0.787	0.186
x	$L_{geom} + L_{color} + L_{sem}$ (w/o min.)	18.28	0.784	0.194
xi	$L_{geom} + L_{color} + L_{sem}$ (single-stage)	18.15	0.783	0.186
xii	$L_{geom} + L_{color} + L_{sem}$ (w/o matching)	16.05	0.717	0.224
xiii	$L_{geom} + L_{color} + L_{sem}$ (SIFT [17])	16.04	0.704	0.238
xiv	$L_{geom} + L_{color} + L_{sem} + L_{locality}$ (ours)	19.13	0.792	0.186

the low-level features of VGG16 for the semantics constraint, balancing the positive effect from local semantic features and missing details.

Minimum Loss in Consistency Losses. We demonstrate in the row x the effect of the min operation in Eq. (9) - Eq. (11). min softens the constraints imposed on the 3D Gaussians by reducing the influence of errors in feature matching and rendered depth.

Multi-stage Training. Row xi reports results with single-stage training, in which training views and novel views are utilized during optimization. Compared to the multi-stage training in row ix , the single-stage regime performs worse, since the Gaussian parameters tend to overfit to the training views. Moreover, without proper scene initialization, the depth maps for the training views become contaminated by the novel views at the start of the training procedure.

Feature Matching. Experiments are also conducted using only a single known view for the consistency losses in row xii . We utilize a single training view, sample a random novel view in its frustum view, and reproject the points to it for additional supervision. There’s a drastic difference in rendering performance compared to the variant where feature matching is not used in xii . This happens because the rendered depth in a training view may contain many errors that mislead the novel view synthesis. Feature matching algorithm plays an important role by choosing points appearing in several views for the warping, providing the ability to compute the agreement mask for filtering out unreliable color, depth, and features. RoMa [9] is particularly effective since it provides many correspondences between the images that are quite far from each other. Experiments are conducted with a classical feature matching algorithm [17] in $xiii$, but it fails due to a limited number of matches (see Fig. 7).

5 Conclusion

We introduced **FewViewGS**, a few-shot novel view synthesis system based on 3D Gaussian Splatting as the scene representation that enables accurate renderings using only a handful of training images. We proposed an effective multi-stage training scheme, novel view consistency constraints, and regularization losses. Compared to previous state-of-the-art sparse novel view synthesis systems, we achieve high-quality rendering without relying on complex priors like depth estimation or diffusion models. We demonstrated that **FewViewGS** yields compelling results in rendering on both real-world and synthetic datasets.

Limitations. Our method may struggle to render texture-rich regions accurately, particularly when novel views diverge significantly from the input views. Additionally, as indicated by our ablation study, utilizing a more precise feature-matching network to create dense matched pairs would be beneficial, as this can offer more robust supervision for the novel views.

Acknowledgement

Ruihong Yin is financially supported by China Scholarship Council and University of Amsterdam. Vladimir Yugay and Yue Li are financially supported by TomTom, the University of Amsterdam and the allowance of Top consortia for Knowledge and Innovation (TKIs) from the Netherlands Ministry of Economic Affairs and Climate Policy.

References

- [1] Barron, J.T., Mildenhall, B., Tancik, M., Hedman, P., Martin-Brualla, R., Srinivasan, P.P.: Mip-nerf: A multiscale representation for anti-aliasing neural radiance fields. In: Proceedings of the IEEE/CVF International Conference on Computer Vision. pp. 5855–5864 (2021)
- [2] Chen, A., Xu, Z., Geiger, A., Yu, J., Su, H.: Tensorf: Tensorial radiance fields. In: European Conference on Computer Vision. pp. 333–350. Springer (2022)
- [3] Chen, A., Xu, Z., Zhao, F., Zhang, X., Xiang, F., Yu, J., Su, H.: Mvsnerf: Fast generalizable radiance field reconstruction from multi-view stereo. In: Proceedings of the IEEE/CVF International Conference on Computer Vision. pp. 14124–14133 (2021)
- [4] Chen, D., Liu, Y., Huang, L., Wang, B., Pan, P.: Geoaug: Data augmentation for few-shot nerf with geometry constraints. In: European Conference on Computer Vision. pp. 322–337. Springer (2022)
- [5] Chibane, J., Bansal, A., Lazova, V., Pons-Moll, G.: Stereo radiance fields (srf): Learning view synthesis for sparse views of novel scenes. In: Proceedings of the IEEE/CVF Conference on Computer Vision and Pattern Recognition. pp. 7911–7920 (2021)
- [6] Chung, J., Oh, J., Lee, K.M.: Depth-regularized optimization for 3d gaussian splatting in few-shot images. In: Proceedings of the IEEE/CVF Conference on Computer Vision and Pattern Recognition. pp. 811–820 (2024)
- [7] Dagli, R., Hibi, A., Krishnan, R.G., Tyrrell, P.N.: Nerf-us: Removing ultrasound imaging artifacts from neural radiance fields in the wild. arXiv preprint arXiv:2408.10258 (2024)
- [8] Deng, K., Liu, A., Zhu, J.Y., Ramanan, D.: Depth-supervised nerf: Fewer views and faster training for free. In: Proceedings of the IEEE/CVF Conference on Computer Vision and Pattern Recognition. pp. 12882–12891 (2022)
- [9] Edstedt, J., Sun, Q., Bökman, G., Wadenbäck, M., Felsberg, M.: Roma: Robust dense feature matching. In: Proceedings of the IEEE/CVF Conference on Computer Vision and Pattern Recognition. pp. 19790–19800 (2024)
- [10] Garbin, S.J., Kowalski, M., Johnson, M., Shotton, J., Valentin, J.: Fastnerf: High-fidelity neural rendering at 200fps. In: Proceedings of the IEEE/CVF International Conference on Computer Vision. pp. 14346–14355 (2021)
- [11] Jain, A., Tancik, M., Abbeel, P.: Putting nerf on a diet: Semantically consistent few-shot view synthesis. In: Proceedings of the IEEE/CVF International Conference on Computer Vision. pp. 5885–5894 (2021)
- [12] Jensen, R., Dahl, A.L., Vogiatzis, G., Tola, E., Aanaes, H.: Large scale multi-view stereopsis evaluation. Proceedings of the IEEE/CVF Conference on Computer Vision and Pattern Recognition pp. 406–413 (2014)
- [13] Kerbl, B., Kopanas, G., Leimkühler, T., Drettakis, G.: 3d gaussian splatting for real-time radiance field rendering. *ACM Transactions on Graphics* **42**(4), 139–1 (2023)
- [14] Kosiorek, A.R., Strathmann, H., Zoran, D., Moreno, P., Schneider, R., Mokra, S., Rezende, D.J.: Nerf-vae: A geometry aware 3d scene generative model. In: International Conference on Machine Learning. pp. 5742–5752. PMLR (2021)
- [15] Li, J., Zhang, J., Bai, X., Zheng, J., Ning, X., Zhou, J., Gu, L.: Dngaussian: Optimizing sparse-view 3d gaussian radiance fields with global-local depth normalization. In: Proceedings of the IEEE/CVF Conference on Computer Vision and Pattern Recognition. pp. 20775–20785 (2024)

- [16] Liu, L., Li, J., Zollhöfer, M., Shuai, Q., Dai, A., Lovegrove, S., Theobalt, C.: Neural actor: Neural free-view synthesis of human actors with pose control. In: *ACM Transactions on Graphics*. vol. 40, pp. 1–16. ACM (2021)
- [17] Lowe, D.G.: Distinctive image features from scale-invariant keypoints. *International Journal of Computer Vision* **60**, 91–110 (2004)
- [18] Martin-Brualla, R., Radwan, N., Sajjadi, M.S., Barron, J.T., Dosovitskiy, A., Duckworth, D.: Nerf in the wild: Neural radiance fields for unconstrained photo collections. In: *Proceedings of the IEEE/CVF Conference on Computer Vision and Pattern Recognition*. pp. 7210–7219 (2021)
- [19] Mildenhall, B., Srinivasan, P.P., Ortiz-Cayon, R., Kalantari, N.K., Ramamoorthi, R., Ng, R., Kar, O.: Local light field fusion: Practical view synthesis with prescriptive sampling guidelines. In: *ACM Transactions on Graphics*. vol. 38, pp. 1–14. ACM New York, NY, USA (2019)
- [20] Mildenhall, B., Srinivasan, P.P., Tancik, M., Barron, J.T., Ramamoorthi, R., Ng, R.: Nerf: Representing scenes as neural radiance fields for view synthesis. *Communications of the ACM* **65**(1), 99–106 (2021)
- [21] Müller, T., Evans, A., Schied, C., Keller, A.: Instant neural graphics primitives with a multiresolution hash encoding. *ACM Transactions on Graphics* **41**(4), 1–15 (2022)
- [22] Niemeyer, M., Barron, J.T., Mildenhall, B., Sajjadi, M.S., Geiger, A., Radwan, N.: Regnerf: Regularizing neural radiance fields for view synthesis from sparse inputs. In: *Proceedings of the IEEE/CVF Conference on Computer Vision and Pattern Recognition*. pp. 5480–5490 (2022)
- [23] Oquab, M., Darcet, T., Moutakanni, T., Vo, H., Szafraniec, M., Khalidov, V., Fernandez, P., Haziza, D., Massa, F., El-Nouby, A., et al.: Dinov2: Learning robust visual features without supervision. *arXiv preprint arXiv:2304.07193* (2023)
- [24] Paliwal, A., Ye, W., Xiong, J., Kotovenko, D., Ranjan, R., Chandra, V., Kalantari, N.K.: Coherentgs: Sparse novel view synthesis with coherent 3d gaussians. *arXiv preprint arXiv:2403.19495* (2024)
- [25] Peng, S., Dong, J., Wang, Q., Zhang, S., Shuai, Q., Bao, H., Zhou, X.: Animatable neural radiance fields for modeling dynamic human bodies. In: *Proceedings of the IEEE/CVF International Conference on Computer Vision*. pp. 14314–14323 (2021)
- [26] Peng, S., Xu, Y., Wang, Q., Jiang, Q.S., Bao, H., Zhou, X.: Neural body: Implicit neural representations with structured latent codes for novel view synthesis of dynamic humans. In: *Proceedings of the IEEE/CVF Conference on Computer Vision and Pattern Recognition*. pp. 9054–9063 (2021)
- [27] Radford, A., Kim, J.W., Hallacy, C., Ramesh, A., Goh, G., Agarwal, S., Sastry, G., Askell, A., Mishkin, P., Clark, J., et al.: Learning transferable visual models from natural language supervision. In: *International Conference on Machine Learning*. pp. 8748–8763. PMLR (2021)
- [28] Rosinol, A., Leonard, J.J., Carlone, L.: Nerf-slam: Real-time dense monocular slam with neural radiance fields. In: *IEEE/RSJ International Conference on Intelligent Robots and Systems*. pp. 3437–3444. IEEE (2023)
- [29] Schonberger, J.L., Frahm, J.M.: Structure-from-motion revisited. In: *Proceedings of the IEEE/CVF Conference on Computer Vision and Pattern Recognition*. pp. 4104–4113 (2016)
- [30] Simonyan, K., Zisserman, A.: Very deep convolutional networks for large-scale image recognition. *arXiv preprint arXiv:1409.1556* (2015)
- [31] Somraj, N., Soundararajan, R.: Vip-nerf: Visibility prior for sparse input neural radiance fields. In: *ACM SIGGRAPH 2023 Conference Proceedings*. pp. 1–11 (2023)
- [32] Svitov, D., Morerio, P., Agapito, L., Del Bue, A.: Haha: Highly articulated gaussian human avatars with textured mesh prior. *arXiv preprint arXiv:2404.01053* (2024)

- [33] Truong, P., Rakotosaona, M.J., Manhardt, F., Tombari, F.: Sparf: Neural radiance fields from sparse and noisy poses. In: Proceedings of the IEEE/CVF Conference on Computer Vision and Pattern Recognition. pp. 4190–4200 (2023)
- [34] Wang, G., Chen, Z., Loy, C.C., Liu, Z.: Sparsenerf: Distilling depth ranking for few-shot novel view synthesis. In: Proceedings of the IEEE/CVF International Conference on Computer Vision. pp. 9065–9076 (2023)
- [35] Wang, Z., Bovik, A.C., Sheikh, H.R., Simoncelli, E.P.: Image quality assessment: from error visibility to structural similarity. *IEEE Transactions on Image Processing* **13**(4), 600–612 (2004)
- [36] Weng, C.Y., Curless, B., Srinivasan, P.P., Barron, J.T., Kemelmacher-Shlizerman, I.: Humannerf: Free-viewpoint rendering of moving people from monocular video. In: Proceedings of the IEEE/CVF Conference on Computer Vision and Pattern Recognition. pp. 16210–16220 (2022)
- [37] Wynn, J., Turmukhambetov, D.: Diffusionerf: Regularizing neural radiance fields with denoising diffusion models. In: Proceedings of the IEEE/CVF Conference on Computer Vision and Pattern Recognition. pp. 4180–4189 (2023)
- [38] Xiong, H., Muttukuru, S., Upadhyay, R., Chari, P., Kadambi, A.: Sparsegts: Real-time 360 degree sparse view synthesis using gaussian splatting. *arXiv preprint arXiv:2312.00206* (2023)
- [39] Yang, C., Li, P., Zhou, Z., Yuan, S., Liu, B., Yang, X., Qiu, W., Shen, W.: Nerfvs: Neural radiance fields for free view synthesis via geometry scaffolds. In: Proceedings of the IEEE/CVF Conference on Computer Vision and Pattern Recognition. pp. 16549–16558 (2023)
- [40] Yang, J., Pavone, M., Wang, Y.: Freenerf: Improving few-shot neural rendering with free frequency regularization. In: Proceedings of the IEEE/CVF Conference on Computer Vision and Pattern Recognition. pp. 8254–8263 (2023)
- [41] Yen-Chen, L., Florence, P., Yu, A.Z., Duong, D., Rodriguez, A.: inerf: Inverting neural radiance fields for pose estimation. In: *IEEE/RSJ International Conference on Intelligent Robots and Systems*. pp. 1323–1330 (2020)
- [42] Yu, A., Li, V.Y., Tancik, M., Kanazawa, A.: Plenotrees for real-time rendering of neural radiance fields. In: Proceedings of the IEEE/CVF International Conference on Computer Vision. pp. 5752–5761 (2021)
- [43] Yu, A., Ye, V., Tancik, M., Kanazawa, A.: pixelnerf: Neural radiance fields from one or few images. In: Proceedings of the IEEE/CVF Conference on Computer Vision and Pattern Recognition. pp. 4578–4587 (2021)
- [44] Yugay, V., Li, Y., Gevers, T., Oswald, M.R.: Gaussian-slam: Photo-realistic dense slam with gaussian splatting. *arXiv preprint arXiv:2312.10070* (2024)
- [45] Zhang, R., Isola, P., Efros, A.A., Shechtman, E., Wang, O.: The unreasonable effectiveness of deep features as a perceptual metric. In: Proceedings of the IEEE/CVF Conference on Computer Vision and Pattern Recognition. pp. 586–595 (2018)
- [46] Zhu, Z., Fan, Z., Jiang, Y., Wang, Z.: Fsgs: Real-time few-shot view synthesis using gaussian splatting. In: *European Conference on Computer Vision*. pp. 145–163. Springer (2025)
- [47] Zwicker, M., Pfister, H., Van Baar, J., Gross, M.: Surface splatting. In: Proceedings of the 28th Annual Conference on Computer Graphics and Interactive Techniques. pp. 371–378 (2001)

A Appendix

A.1 Additional Quantitative Results

Comparison with SOTA methods under 6-view and 9-view settings. The results for 6-view and 9-view settings are given in Tab. 5. Our method shows improved performance over the baseline 3DGS with both SFM and random initialization. Notably, with SFM initialization, our method surpasses NeRF-based methods on both datasets.

Comparison with SOTA methods on training and inference time. Tab. 11 displays the training time on a single NVIDIA A6000 GPU under 3-view setting on DTU. Our method demonstrates comparable training time and is faster than SparseGS [38] (which uses a pre-trained diffusion model) and FSGS [46] (which relies on a pre-trained depth network). For inference time, since all methods utilize the same rendering process as 3DGS, their inference time is similar across these methods, at around 300 FPS.

Ablation study for hyperparameters. We provide evaluations for hyperparameters and the multi-stage settings in Tab. 6 - Tab. 10 on DTU with 3 training views. (1) α in Eq. (12): we set it to a low weight due to the lack of ground truth for the depth. It can be seen that, in Tab. 7, larger (e.g. 0.2) gets poorer results, primarily due to noise in predicted depth values. (2) β in Eq. (12): due to the importance of color supervision for the novel view synthesis, a large weight is utilized in the experiment. In Tab. 6, a value of 0.5 achieves the best performance. (3) γ in Eq. (12): The results in Tab. 9 demonstrate that our method is robust to different γ values, with $\gamma = 0.001$ being optimal. (4) η in Eq. (15): The pre-training loss in the intermediate stage is employed to ensure sufficient supervision for novel views. In Tab. 8, a lower η (0.01) does not solve this very well, while higher η (0.1 and 0.5) fails to prevent overfitting to the training views. (5) Multi-stage settings: we evaluate the influence of iterations for each stage in our 3-stage training in Tab. 10. The last two rows show that a fewer/more iteration in the first stage leads to worse results, due to underfitting/overfitting to training views. The 1st-5th rows demonstrate that the fine-tuning stage enhances performance and achieves optimal results with 500 iterations.

Table 5: Quantitative evaluation on LLFF and DTU under 6-view and 9-view settings.

Setting	Init.	6-view (LLFF)			9-view (LLFF)			
		PSNR \uparrow	SSIM \uparrow	LPIPS \downarrow	PSNR \uparrow	SSIM \uparrow	LPIPS \downarrow	
SRF	-	13.10	0.293	0.594	13.00	0.297	0.605	
PixelNeRF	Trained on DTU	-	8.74	0.280	0.676	8.61	0.274	0.665
MVSNeRF		-	19.79	0.656	0.269	20.47	0.689	0.242
Mip-NeRF		-	20.87	0.692	0.255	24.26	0.805	0.172
DietNeRF	Optimized per Scene	-	21.75	0.717	0.248	24.28	0.801	0.183
RegNeRF		-	23.10	0.760	0.206	24.86	0.820	0.161
FreeNeRF		-	23.73	0.779	0.195	25.13	0.827	0.160
3DGS	Optimized per Scene	Random	19.81	0.638	0.245	22.32	0.753	0.169
Ours		Random	21.33	0.688	0.220	23.09	0.769	0.164
3DGS	Optimized per Scene	SFM	23.65	0.807	0.123	25.26	0.852	0.096
Ours		SFM	24.35	0.826	0.126	25.90	0.868	0.095

Setting	Init.	6-view (DTU)			9-view (DTU)			
		PSNR \uparrow	SSIM \uparrow	LPIPS \downarrow	PSNR \uparrow	SSIM \uparrow	LPIPS \downarrow	
SRF	-	17.77	0.616	0.401	18.56	0.652	0.359	
PixelNeRF	Trained on DTU	-	21.02	0.684	0.340	22.23	0.714	0.323
MVSNeRF		-	18.26	0.695	0.321	20.32	0.735	0.280
Mip-NeRF		-	14.33	0.568	0.394	20.71	0.799	0.209
DietNeRF	Optimized per Scene	-	18.70	0.668	0.336	22.16	0.740	0.277
RegNeRF		-	19.10	0.757	0.233	22.30	0.823	0.184
FreeNeRF		-	22.39	0.779	0.240	24.20	0.833	0.187
3DGS	Optimized per Scene	Random	20.46	0.824	0.145	24.75	0.914	0.076
Ours		Random	23.51	0.891	0.123	25.75	0.925	0.101
3DGS	Optimized per Scene	SFM	23.63	0.912	0.074	26.53	0.946	0.047
Ours		SFM	24.33	0.920	0.069	27.31	0.953	0.041

Table 6: Ablation study for the hyperparameter β in Eq. (12).

β	PSNR \uparrow	SSIM \uparrow	LPIPS \downarrow
0.1	18.68	0.785	0.186
0.5	19.13	0.792	0.186
1.0	18.70	0.784	0.191

Table 7: Ablation study for the hyperparameter α in Eq. (12).

α	PSNR \uparrow	SSIM \uparrow	LPIPS \downarrow
0.01	18.67	0.778	0.192
0.05	19.13	0.792	0.186
0.1	18.92	0.790	0.190
0.2	18.50	0.786	0.196

Table 8: Ablation study for the hyperparameter η in Eq. (15).

η	PSNR \uparrow	SSIM \uparrow	LPIPS \downarrow
0.01	18.89	0.781	0.201
0.05	19.13	0.792	0.186
0.1	18.58	0.785	0.183
0.5	18.20	0.772	0.179

Table 9: Ablation study for the hyperparameter γ in Eq. (12).

γ	PSNR \uparrow	SSIM \uparrow	LPIPS \downarrow
0.001	19.13	0.792	0.186
0.01	18.84	0.785	0.186
0.1	18.85	0.787	0.187
0.5	19.03	0.792	0.184
1.0	18.88	0.789	0.188

Table 10: Ablation study for the multi-stage settings.

1st	2nd	3rd	PSNR \uparrow	SSIM \uparrow	LPIPS \downarrow
2000	8000	0	18.49	0.782	0.195
2000	7500	0	18.37	0.782	0.198
2000	7200	800	18.85	0.787	0.187
2000	7500	500	19.13	0.792	0.186
2000	7800	200	18.71	0.786	0.191
1000	8500	500	18.72	0.772	0.228
3000	6500	500	18.76	0.782	0.189

Table 11: Comparison of training time.

Method	Time \downarrow
3DGS	1.17 min
SparseGS	51.78 min
DNGaussian	2.65 min
FSGS	10.90 min
Ours	5.82 min

A.2 Additional Qualitative Results

Visualization of unseen regions. In Fig. 3, we compare the results of unseen regions between our method and FSGS [46]. The visualization shows that our method produces fewer artifacts and outperforms FSGS (which relies on a pre-trained depth network). This improvement is due to our multi-view consistency constraints, which offer accurate supervision for seen regions, while the proposed locality-preserving regularization maintains local smoothness and reduces artifacts.

Visualization of predicted depth. Fig. 4 presents the generated depth by 3DGS [13] and our method. Our method produces clearer and more accurate depth estimations than the baseline 3DGS, demonstrating its effectiveness.

Ablation study on multi-view constraints. In Fig. 5, qualitative results are shown of our proposed multi-view geometry, color, and semantic constraints. The results indicate that each design choice contributes to improved rendering quality.

Ablation study on various networks for semantic feature extraction. Fig. 6 compares our results (VGG16) with DINOv2 and CLIP. The results indicate that DINOv2 and CLIP introduce substantial noise, particularly in boundary regions, and detail preservation is hindered by feature down-sampling in both models.

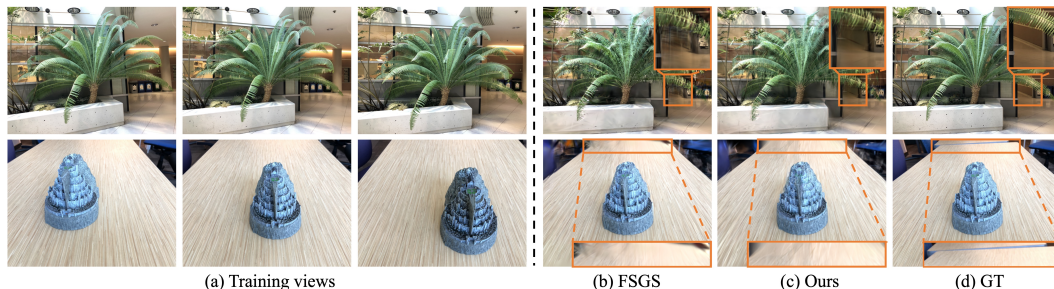


Figure 3: **Visualizations for unseen regions.** The orange regions are not observed in the training views. Compared to FSGS [46], our method generates better results and fewer artifacts.

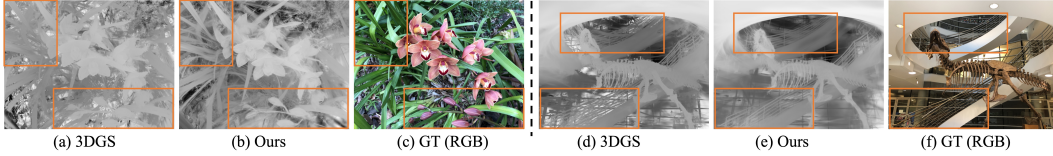


Figure 4: **Visualizations for predicted depth.** Compared to the baseline 3DGS [13], our method yields more accurate depth values.

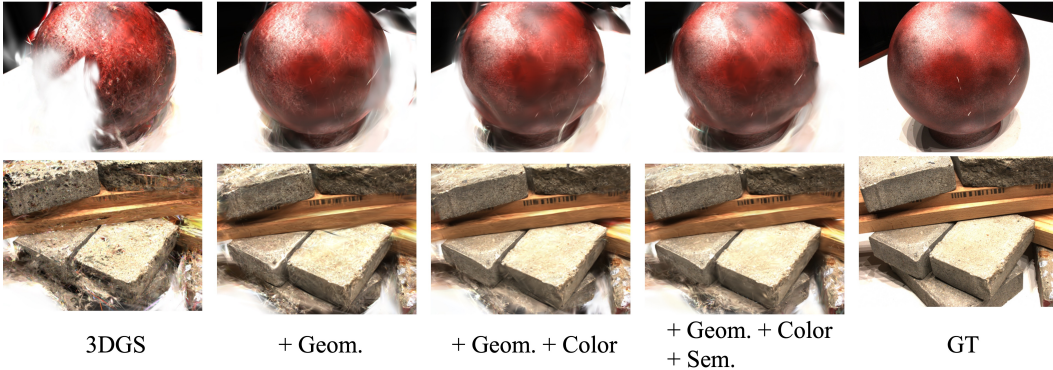


Figure 5: Comparison of the results with our proposed multi-view alignment.

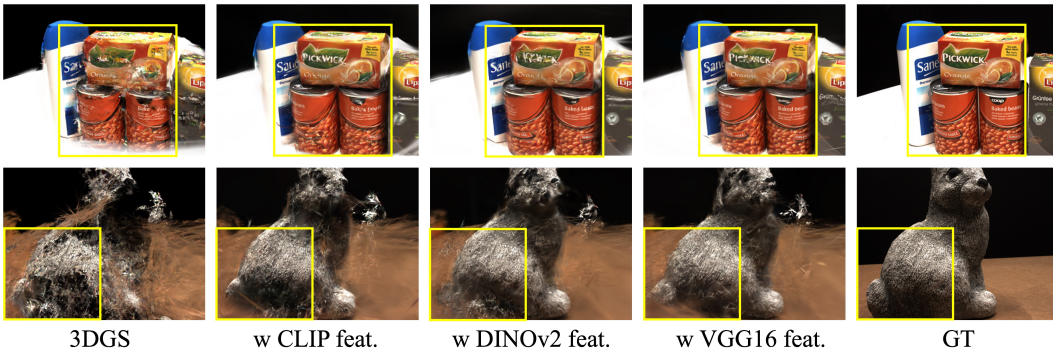


Figure 6: Comparison of the results with different feature networks.



Figure 7: Comparison of the matched results with different feature-matching algorithms. Roma[9] and SIFT[17] implement feature matching between the *Image1* and *Image2*.

Ablation study on feature matching. In Fig. 8, the results with and without feature matching are presented. It is shown that the model without feature matching generates false surfaces due to noise in the multi-view projection.

In Fig. 7, we show the difference between matching results generated by RoMa and SIFT. RoMa produces denser and more accurate matches than SIFT, which significantly enhances the model's performance when using RoMa.

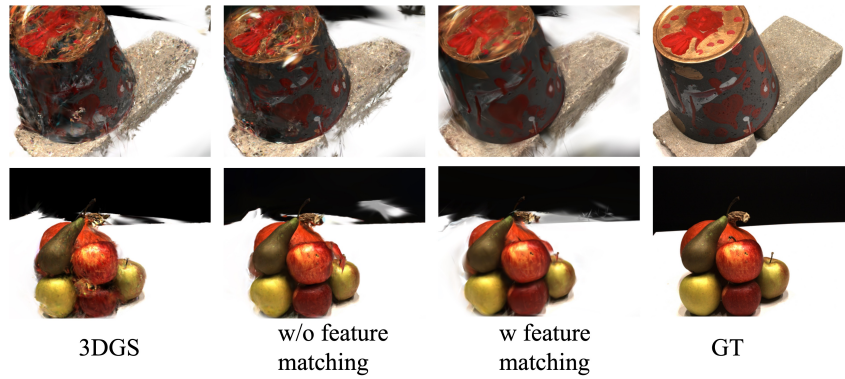


Figure 8: Comparison of the results without and with feature matching results.

Ablation study on multi-stage training. The comparison between single-stage and multi-stage training is demonstrated in Fig. 9. Single-stage training results in blurry views due to inaccurate depth rendering in the early training stages, leading to errors in multi-view projection.



Figure 9: Comparison between single-stage and multi-stage training with our multi-view consistency constraints.

NeurIPS Paper Checklist

1. Claims

Question: Do the main claims made in the abstract and introduction accurately reflect the paper's contributions and scope?

Answer: [Yes]

Justification: We highlight our novel multi-stage training scheme and correspondence-driven losses on sampled novel views which greatly improves the final NVS results.

Guidelines:

- The answer NA means that the abstract and introduction do not include the claims made in the paper.
- The abstract and/or introduction should clearly state the claims made, including the contributions made in the paper and important assumptions and limitations. A No or NA answer to this question will not be perceived well by the reviewers.
- The claims made should match theoretical and experimental results, and reflect how much the results can be expected to generalize to other settings.
- It is fine to include aspirational goals as motivation as long as it is clear that these goals are not attained by the paper.

2. Limitations

Question: Does the paper discuss the limitations of the work performed by the authors?

Answer: [Yes]

Justification: We address the limitation of our method at the end of Sec. 5.

Guidelines:

- The answer NA means that the paper has no limitation while the answer No means that the paper has limitations, but those are not discussed in the paper.
- The authors are encouraged to create a separate "Limitations" section in their paper.
- The paper should point out any strong assumptions and how robust the results are to violations of these assumptions (e.g., independence assumptions, noiseless settings, model well-specification, asymptotic approximations only holding locally). The authors should reflect on how these assumptions might be violated in practice and what the implications would be.
- The authors should reflect on the scope of the claims made, e.g., if the approach was only tested on a few datasets or with a few runs. In general, empirical results often depend on implicit assumptions, which should be articulated.
- The authors should reflect on the factors that influence the performance of the approach. For example, a facial recognition algorithm may perform poorly when image resolution is low or images are taken in low lighting. Or a speech-to-text system might not be used reliably to provide closed captions for online lectures because it fails to handle technical jargon.
- The authors should discuss the computational efficiency of the proposed algorithms and how they scale with dataset size.
- If applicable, the authors should discuss possible limitations of their approach to address problems of privacy and fairness.
- While the authors might fear that complete honesty about limitations might be used by reviewers as grounds for rejection, a worse outcome might be that reviewers discover limitations that aren't acknowledged in the paper. The authors should use their best judgment and recognize that individual actions in favor of transparency play an important role in developing norms that preserve the integrity of the community. Reviewers will be specifically instructed to not penalize honesty concerning limitations.

3. Theory Assumptions and Proofs

Question: For each theoretical result, does the paper provide the full set of assumptions and a complete (and correct) proof?

Answer: [NA]

Justification: Our method does not contribute on theoretical results.

Guidelines:

- The answer NA means that the paper does not include theoretical results.
- All the theorems, formulas, and proofs in the paper should be numbered and cross-referenced.
- All assumptions should be clearly stated or referenced in the statement of any theorems.
- The proofs can either appear in the main paper or the supplemental material, but if they appear in the supplemental material, the authors are encouraged to provide a short proof sketch to provide intuition.
- Inversely, any informal proof provided in the core of the paper should be complemented by formal proofs provided in appendix or supplemental material.
- Theorems and Lemmas that the proof relies upon should be properly referenced.

4. Experimental Result Reproducibility

Question: Does the paper fully disclose all the information needed to reproduce the main experimental results of the paper to the extent that it affects the main claims and/or conclusions of the paper (regardless of whether the code and data are provided or not)?

Answer: [Yes]

Justification: We provide detailed method and hyperparameter settings in Sec. 3 and Sec. 4. Our experiments in Sec. 4 are all using publicly available datasets.

Guidelines:

- The answer NA means that the paper does not include experiments.
- If the paper includes experiments, a No answer to this question will not be perceived well by the reviewers: Making the paper reproducible is important, regardless of whether the code and data are provided or not.
- If the contribution is a dataset and/or model, the authors should describe the steps taken to make their results reproducible or verifiable.
- Depending on the contribution, reproducibility can be accomplished in various ways. For example, if the contribution is a novel architecture, describing the architecture fully might suffice, or if the contribution is a specific model and empirical evaluation, it may be necessary to either make it possible for others to replicate the model with the same dataset, or provide access to the model. In general, releasing code and data is often one good way to accomplish this, but reproducibility can also be provided via detailed instructions for how to replicate the results, access to a hosted model (e.g., in the case of a large language model), releasing of a model checkpoint, or other means that are appropriate to the research performed.
- While NeurIPS does not require releasing code, the conference does require all submissions to provide some reasonable avenue for reproducibility, which may depend on the nature of the contribution. For example
 - (a) If the contribution is primarily a new algorithm, the paper should make it clear how to reproduce that algorithm.
 - (b) If the contribution is primarily a new model architecture, the paper should describe the architecture clearly and fully.
 - (c) If the contribution is a new model (e.g., a large language model), then there should either be a way to access this model for reproducing the results or a way to reproduce the model (e.g., with an open-source dataset or instructions for how to construct the dataset).
 - (d) We recognize that reproducibility may be tricky in some cases, in which case authors are welcome to describe the particular way they provide for reproducibility. In the case of closed-source models, it may be that access to the model is limited in some way (e.g., to registered users), but it should be possible for other researchers to have some path to reproducing or verifying the results.

5. Open access to data and code

Question: Does the paper provide open access to the data and code, with sufficient instructions to faithfully reproduce the main experimental results, as described in supplemental material?

Answer: [Yes]

Justification: We use publicly available datasets and will open source our code later with instructions on how to run the experiments we reported in Sec. 4.

Guidelines:

- The answer NA means that paper does not include experiments requiring code.
- Please see the NeurIPS code and data submission guidelines (<https://nips.cc/public/guides/CodeSubmissionPolicy>) for more details.
- While we encourage the release of code and data, we understand that this might not be possible, so “No” is an acceptable answer. Papers cannot be rejected simply for not including code, unless this is central to the contribution (e.g., for a new open-source benchmark).
- The instructions should contain the exact command and environment needed to run to reproduce the results. See the NeurIPS code and data submission guidelines (<https://nips.cc/public/guides/CodeSubmissionPolicy>) for more details.
- The authors should provide instructions on data access and preparation, including how to access the raw data, preprocessed data, intermediate data, and generated data, etc.
- The authors should provide scripts to reproduce all experimental results for the new proposed method and baselines. If only a subset of experiments are reproducible, they should state which ones are omitted from the script and why.
- At submission time, to preserve anonymity, the authors should release anonymized versions (if applicable).
- Providing as much information as possible in supplemental material (appended to the paper) is recommended, but including URLs to data and code is permitted.

6. Experimental Setting/Details

Question: Does the paper specify all the training and test details (e.g., data splits, hyperparameters, how they were chosen, type of optimizer, etc.) necessary to understand the results?

Answer: [Yes]

Justification: We have described the dataset splits and hyperparameters in detail in the experiments section Sec. 4.

Guidelines:

- The answer NA means that the paper does not include experiments.
- The experimental setting should be presented in the core of the paper to a level of detail that is necessary to appreciate the results and make sense of them.
- The full details can be provided either with the code, in appendix, or as supplemental material.

7. Experiment Statistical Significance

Question: Does the paper report error bars suitably and correctly defined or other appropriate information about the statistical significance of the experiments?

Answer: [No]

Justification: We haven't reported experiment results with error bars.

Guidelines:

- The answer NA means that the paper does not include experiments.
- The authors should answer "Yes" if the results are accompanied by error bars, confidence intervals, or statistical significance tests, at least for the experiments that support the main claims of the paper.
- The factors of variability that the error bars are capturing should be clearly stated (for example, train/test split, initialization, random drawing of some parameter, or overall run with given experimental conditions).
- The method for calculating the error bars should be explained (closed form formula, call to a library function, bootstrap, etc.)
- The assumptions made should be given (e.g., Normally distributed errors).

- It should be clear whether the error bar is the standard deviation or the standard error of the mean.
- It is OK to report 1-sigma error bars, but one should state it. The authors should preferably report a 2-sigma error bar than state that they have a 96% CI, if the hypothesis of Normality of errors is not verified.
- For asymmetric distributions, the authors should be careful not to show in tables or figures symmetric error bars that would yield results that are out of range (e.g. negative error rates).
- If error bars are reported in tables or plots, The authors should explain in the text how they were calculated and reference the corresponding figures or tables in the text.

8. Experiments Compute Resources

Question: For each experiment, does the paper provide sufficient information on the computer resources (type of compute workers, memory, time of execution) needed to reproduce the experiments?

Answer: [Yes]

Justification: We have included the number and model of GPU that we used in experiments section Sec. 4.

Guidelines:

- The answer NA means that the paper does not include experiments.
- The paper should indicate the type of compute workers CPU or GPU, internal cluster, or cloud provider, including relevant memory and storage.
- The paper should provide the amount of compute required for each of the individual experimental runs as well as estimate the total compute.
- The paper should disclose whether the full research project required more compute than the experiments reported in the paper (e.g., preliminary or failed experiments that didn't make it into the paper).

9. Code Of Ethics

Question: Does the research conducted in the paper conform, in every respect, with the NeurIPS Code of Ethics <https://neurips.cc/public/EthicsGuidelines>?

Answer: [Yes]

Justification: Our research conforms with the NeurIPS Code of Ethics.

Guidelines:

- The answer NA means that the authors have not reviewed the NeurIPS Code of Ethics.
- If the authors answer No, they should explain the special circumstances that require a deviation from the Code of Ethics.
- The authors should make sure to preserve anonymity (e.g., if there is a special consideration due to laws or regulations in their jurisdiction).

10. Broader Impacts

Question: Does the paper discuss both potential positive societal impacts and negative societal impacts of the work performed?

Answer: [NA]

Justification: Our method focuses on the research topic few-show novel view synthesis, which poses no noticeable societal impact.

Guidelines:

- The answer NA means that there is no societal impact of the work performed.
- If the authors answer NA or No, they should explain why their work has no societal impact or why the paper does not address societal impact.
- Examples of negative societal impacts include potential malicious or unintended uses (e.g., disinformation, generating fake profiles, surveillance), fairness considerations (e.g., deployment of technologies that could make decisions that unfairly impact specific groups), privacy considerations, and security considerations.

- The conference expects that many papers will be foundational research and not tied to particular applications, let alone deployments. However, if there is a direct path to any negative applications, the authors should point it out. For example, it is legitimate to point out that an improvement in the quality of generative models could be used to generate deepfakes for disinformation. On the other hand, it is not needed to point out that a generic algorithm for optimizing neural networks could enable people to train models that generate Deepfakes faster.
- The authors should consider possible harms that could arise when the technology is being used as intended and functioning correctly, harms that could arise when the technology is being used as intended but gives incorrect results, and harms following from (intentional or unintentional) misuse of the technology.
- If there are negative societal impacts, the authors could also discuss possible mitigation strategies (e.g., gated release of models, providing defenses in addition to attacks, mechanisms for monitoring misuse, mechanisms to monitor how a system learns from feedback over time, improving the efficiency and accessibility of ML).

11. Safeguards

Question: Does the paper describe safeguards that have been put in place for responsible release of data or models that have a high risk for misuse (e.g., pretrained language models, image generators, or scraped datasets)?

Answer: [NA]

Justification: Our few-shot novel view synthesis pipeline generates results that are scene-specific and does not pose such risk.

Guidelines:

- The answer NA means that the paper poses no such risks.
- Released models that have a high risk for misuse or dual-use should be released with necessary safeguards to allow for controlled use of the model, for example by requiring that users adhere to usage guidelines or restrictions to access the model or implementing safety filters.
- Datasets that have been scraped from the Internet could pose safety risks. The authors should describe how they avoided releasing unsafe images.
- We recognize that providing effective safeguards is challenging, and many papers do not require this, but we encourage authors to take this into account and make a best faith effort.

12. Licenses for existing assets

Question: Are the creators or original owners of assets (e.g., code, data, models), used in the paper, properly credited and are the license and terms of use explicitly mentioned and properly respected?

Answer: [Yes]

Justification: We have included and cited all the datasets and methods we have used in our pipeline, also we have checked that their licenses are suitable for research purpose.

Guidelines:

- The answer NA means that the paper does not use existing assets.
- The authors should cite the original paper that produced the code package or dataset.
- The authors should state which version of the asset is used and, if possible, include a URL.
- The name of the license (e.g., CC-BY 4.0) should be included for each asset.
- For scraped data from a particular source (e.g., website), the copyright and terms of service of that source should be provided.
- If assets are released, the license, copyright information, and terms of use in the package should be provided. For popular datasets, paperswithcode.com/datasets has curated licenses for some datasets. Their licensing guide can help determine the license of a dataset.

- For existing datasets that are re-packaged, both the original license and the license of the derived asset (if it has changed) should be provided.
- If this information is not available online, the authors are encouraged to reach out to the asset’s creators.

13. **New Assets**

Question: Are new assets introduced in the paper well documented and is the documentation provided alongside the assets?

Answer: [No]

Justification: We haven’t released our code yet, but we hope to do so as soon as possible. Upon releasing the code, we will provide instructions on how to reproduce the results.

Guidelines:

- The answer NA means that the paper does not release new assets.
- Researchers should communicate the details of the dataset/code/model as part of their submissions via structured templates. This includes details about training, license, limitations, etc.
- The paper should discuss whether and how consent was obtained from people whose asset is used.
- At submission time, remember to anonymize your assets (if applicable). You can either create an anonymized URL or include an anonymized zip file.

14. **Crowdsourcing and Research with Human Subjects**

Question: For crowdsourcing experiments and research with human subjects, does the paper include the full text of instructions given to participants and screenshots, if applicable, as well as details about compensation (if any)?

Answer: [NA]

Justification: Our paper does not involve crowdsourcing nor research with human subjects.

Guidelines:

- The answer NA means that the paper does not involve crowdsourcing nor research with human subjects.
- Including this information in the supplemental material is fine, but if the main contribution of the paper involves human subjects, then as much detail as possible should be included in the main paper.
- According to the NeurIPS Code of Ethics, workers involved in data collection, curation, or other labor should be paid at least the minimum wage in the country of the data collector.

15. **Institutional Review Board (IRB) Approvals or Equivalent for Research with Human Subjects**

Question: Does the paper describe potential risks incurred by study participants, whether such risks were disclosed to the subjects, and whether Institutional Review Board (IRB) approvals (or an equivalent approval/review based on the requirements of your country or institution) were obtained?

Answer: [NA]

Justification: Our paper does not involve crowdsourcing nor research with human subjects.

Guidelines:

- The answer NA means that the paper does not involve crowdsourcing nor research with human subjects.
- Depending on the country in which research is conducted, IRB approval (or equivalent) may be required for any human subjects research. If you obtained IRB approval, you should clearly state this in the paper.
- We recognize that the procedures for this may vary significantly between institutions and locations, and we expect authors to adhere to the NeurIPS Code of Ethics and the guidelines for their institution.
- For initial submissions, do not include any information that would break anonymity (if applicable), such as the institution conducting the review.